

# Enhancing Visible-Infrared Person Re-identification with Modality- and Instance-aware Visual Prompt Learning

Ruiqi Wu\*

School of Computer Science,  
Northwestern Polytechnical  
University  
Xi'an, Shaanxi, China  
Ningbo Institute, Northwestern  
Polytechnical University  
Ningbo, Zhejiang, China  
National Engineering Laboratory for  
Integrated Aero-Space-Ground-Ocean  
Big Data Application Technology  
Xi'an, Shaanxi, China  
wurq@mail.nwpu.edu.cn

Bingliang Jiao\*

School of Computer Science,  
Northwestern Polytechnical  
University  
Xi'an, Shaanxi, China  
Ningbo Institute, Northwestern  
Polytechnical University  
Ningbo, Zhejiang, China  
National Engineering Laboratory for  
Integrated Aero-Space-Ground-Ocean  
Big Data Application Technology  
Xi'an, Shaanxi, China  
bingliang.jiao@mail.nwpu.edu.cn

Wenxuan Wang<sup>†</sup>

School of Computer Science,  
Northwestern Polytechnical  
University  
Xi'an, Shaanxi, China  
Ningbo Institute, Northwestern  
Polytechnical University  
Ningbo, Zhejiang, China  
National Engineering Laboratory for  
Integrated Aero-Space-Ground-Ocean  
Big Data Application Technology  
Xi'an, Shaanxi, China  
wxwang@nwpu.edu.cn

Meng Liu

Honors College, Northwestern  
Polytechnical University  
Xi'an, Shaanxi, China  
School of Electronics and Information,  
Northwestern Polytechnical  
University  
Xi'an, Shaanxi, China  
2020300029@mail.nwpu.edu.cn

Peng Wang

School of Computer Science,  
Northwestern Polytechnical  
University  
Xi'an, Shaanxi, China  
Ningbo Institute, Northwestern  
Polytechnical University  
Ningbo, Zhejiang, China  
National Engineering Laboratory for  
Integrated Aero-Space-Ground-Ocean  
Big Data Application Technology  
Xi'an, Shaanxi, China  
peng.wang@nwpu.edu.cn

## ABSTRACT

The Visible-Infrared Person Re-identification (VI ReID) aims to match visible and infrared images of the same pedestrians across non-overlapped camera views. These two input modalities contain both invariant information, such as shape, and modality-specific details, such as color. An ideal model should utilize valuable information from both modalities during training for enhanced representational capability. However, the gap caused by modality-specific information poses substantial challenges for the VI ReID model to handle distinct modality inputs simultaneously. To address this, we introduce the Modality-aware and Instance-aware Visual Prompts (MIP) network in our work, designed to effectively utilize both invariant and specific information for identification. Specifically, our MIP model is built on the transformer architecture. In this model, we have designed a series of modality-specific prompts, which could enable our model to adapt to and make use of the specific information inherent in different modality inputs, thereby reducing

the interference caused by the modality gap and achieving better identification. Besides, we also employ each pedestrian feature to construct a group of instance-specific prompts. These customized prompts are responsible for guiding our model to adapt to each pedestrian instance dynamically, thereby capturing identity-level discriminative clues for identification. Through extensive experiments on SYSU-MM01 and RegDB datasets, the effectiveness of both our designed modules is evaluated. Additionally, our proposed MIP performs better than most state-of-the-art methods.

## KEYWORDS

Cross-Modality Person Re-Identification, Visible-Infrared Person Re-Identification, Visual Prompt Learning

## ACM Reference Format:

Ruiqi Wu, Bingliang Jiao, Wenxuan Wang, Meng Liu, and Peng Wang. 2024. Enhancing Visible-Infrared Person Re-identification with Modality- and Instance-aware Visual Prompt Learning. In *Proceedings of the 2024 International Conference on Multimedia Retrieval (ICMR '24)*, June 10–14, 2024, Phuket, Thailand. ACM, New York, NY, USA, 11 pages. <https://doi.org/10.1145/3652583.3658109>

\*These authors contributed equally to this work.

<sup>†</sup>Corresponding author.

<sup>‡</sup>This preprint follows the arXiv.org perpetual, non-exclusive license copyright agreement. The final version of this work has been accepted for publication in ICMR'24 by ACM, adhering to the "ACM licensed" copyright agreement. When citing, please refer to the ACM Reference Format.

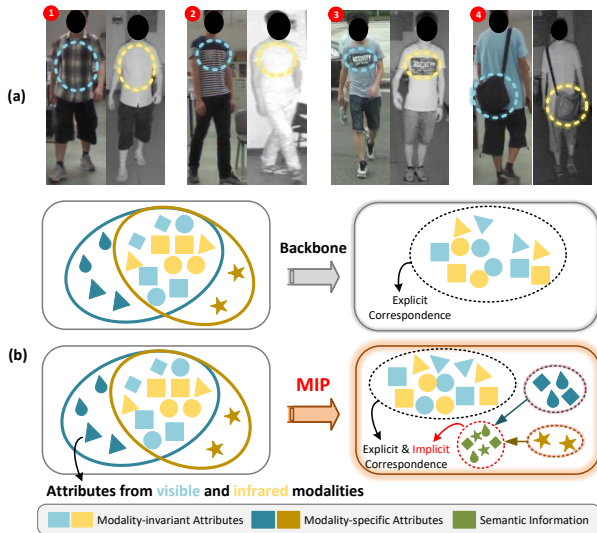


**Figure 1: The illustration of our motivation. (a) Our motivation is to utilize modality-specific details to reveal potential relationships. For example, characteristics like clothing types/materials, discerned from visible images, could influence the heat radiation intensities, thereby impacting infrared brightness variations. For intuitive example, in case 1, a uniform brightness is expected as the striped plaid shirt suggests similar materials. Conversely, Case 3 exhibits varied brightness due to different materials in the T-shirt and logo. (b) Unlike traditional methods emphasizing modality-invariant information while overlooking modality-specific information, our approach integrates modality-specific attributes like color, texture, and brightness to extract and explore potential relationships.**

## 1 INTRODUCTION

Person Re-Identification (ReID) aims to retrieve images of the same individuals across different cameras. Driven by its applications in public security and video surveillance, ReID has garnered significant attention and achieved notable progress. Many existing methods [31, 34, 47, 53] merely focus on the re-identification in daytime scenarios while ignoring the low-light conditions. However, treating ReID as a single-modality problem is unreasonable, which inevitably leads existing methods to fall short in low-light conditions. To address this, infrared cameras have been introduced to capture images for all-day surveillance, leading to the emergence of the Visible-Infrared Person Re-Identification (VI ReID) task.

Different from the visible-visible ReID task, the query and gallery sets in VI ReID are captured by cameras with distinct modalities, resulting in significant modality gaps among the compared person images. To address these modality discrepancies, a straightforward approach involves modality transfer via Generative Adversarial Networks (GAN) [11]. Typically, GAN-based methods [7, 23, 37, 39] are designed to transform images from one modality to another, achieving effective cross-modality matching. However, challenges arise because the brightness of infrared images may not perfectly correspond to the color of visible images [21]. A more general

approach involves extracting discriminative modality-invariant information. For instance, SPOT [3] employs complex multi-level alignment mechanisms and leverages physics knowledge, such as human body structure, to learn discriminative cross-modality invariant features.

Although the existing methods could alleviate the interference caused by the modality gap, they focus on simply eliminating modality-specific information, overlooking the potential utilization of such information. This is unreasonable as there could exist potential correspondences between modality-specific information that could also enhance re-identification [30, 42]. For example, from the clothing types and material, which could be identified from visible images, we can briefly infer the heat radiation intensity of the clothing’s surface. This factor directly influenced the brightness of the corresponding area in infrared images. Intuitively, from the visible image in the first case of Figure 1(a), the pedestrian wears a striped plaid shirt and the material of the different stripes appears to be roughly the same. Based on this, we could expect uniform heat radiation intensities, i.e., uniform brightness in the infrared image, of this upper dress.

Based on this insight, in this work, we aim to make use of both modality-invariant and modality-specific information to achieve better identification, as shown in Figure 1(b). This step is non-trivial, as the modality-specific information inevitably causes the semantic divergence between distinct modality inputs. This divergence makes it challenging for the model to adapt to and process different modality inputs simultaneously. Meanwhile, using separate independent models for different modality inputs is also sub-optimal, as it struggles to fully utilize modality-invariant information, leading to insufficient representational capability. Here, we notice that visual prompts could be a good tool to address this issue. Its extensive use in numerous existing works [1, 4, 15, 27, 44, 54] showcases its ability to preserve the foundational knowledge inherent in the backbone model while adapting models efficiently to various tasks. This inspires us to leverage the visual prompts to learn the modality-invariant information with the backbone model and use a group modality-specific prompt to help the model flexibly adapt and make use of the modality-specific information. Besides, in this work, we also employ each pedestrian feature to construct a group of instance-specific prompts. These customized prompts are responsible for guiding our model to adapt to each pedestrian instance dynamically, thereby capturing discriminative clues for identification.

Specifically, in this paper, we propose a novel and effective Modality-aware and Instance-aware Visual Prompts (MIP) network. The MIP network comprises a global backbone and two prompt learning modules: a Modality-aware Prompt Learning (MPL) module and an Instance-aware Prompt Generator (IPG) module. Initially, we design the MPL module with several learnable prompt vectors. Depending on the modality of inputs, the MPL module provides the backbone with the corresponding modality-specific prompt. Here, the backbone is trained to extract cross-modality consistency information, while the modality-specific prompt guides the backbone to adapt to inputs of different modalities and utilize modality-specific information. Moreover, we have devised an innovative IPG module based on transformer architecture. In this module, we employ a transformer layer to transfer the identity-specific information

from the preliminarily extracted pedestrian features into a group of learnable vectors to construct instance-specific prompts. These prompts are then inserted into the backbone model to direct it to dynamically adapt to the current instance, thereby capturing discriminative clues for identification.

We summarize the contribution of our work as follows:

- We propose a novel VI ReID method, the Modality-aware and Instance-aware Visual Prompts (MIP) network, incorporating visual prompt learning into the VI ReID field.
- We design a Modality-aware Prompt Learning (MPL) module and an Instance-aware Prompt Generator (IPG) to generate modality-specific and instance-specific prompts for the ReID model, which guide the model to adapt to inputs of different modalities and leverage modality-specific information, and capture identity-specific discriminative clues that help re-identification, respectively.
- We execute extensive experiments on VI ReID benchmarks SYSU-MM01 and RegDB, which validate the effectiveness of both our designed modules and demonstrate that MIP performs better than most state-of-the-art methods.

## 2 RELATED WORK

In this section, we briefly review the existing algorithms related to our work in the areas of person re-identification, visible-infrared person re-identification, and visual prompt learning.

### 2.1 Person Re-Identification

Person Re-identification (ReID) is a pivotal task that involves matching query person images with target person images from a gallery image set, attracting considerable attention for its real-world applications and prompting the development of diverse methodologies [5, 12, 16, 17, 28, 32, 34, 36, 43, 48, 53]. Similar tasks include vehicle ReID [25, 38], animal ReID [18], etc.

ReID methods typically comprise two key components: feature representation learning and deep metric learning. Global-based approaches like VLAD [43], BNNeck [28], among others, have been introduced to extract global-level feature representations for individuals' images. Furthermore, part-based methods, such as PCB-RPP [34], leverage part-level clues to amalgamate more robust representations for retrieval purposes. Some algorithms combine both global and local features to exploit their respective advantages. For instance, Wang et al. [36] proposed a multiple granularity network with one branch for global feature representation and two branches for local feature representation. Deep metric learning techniques [5, 12, 48], such as triplet-loss [12] and quadruple-loss [5], aim to increase inter-identity feature distance and reduce intra-identity variation. While many ReID methods excel in visible-visible tasks, they may struggle in low-light scenes due to inadequate handling of substantial domain gaps between visible and infrared modalities. Bridging this gap is crucial to enhance the versatility and applicability of ReID techniques across diverse environmental settings.

### 2.2 Visible-Infrared Person Re-Identification

The Visible-Infrared Person Re-identification (VI ReID) focuses on matching visible and infrared images of the same pedestrians

across cameras. The query and gallery set are captured by cameras with different modalities. However, directly applying visible-visible ReID methods to VI ReID yielded poor results due to modality discrepancies and distinct distribution between modalities [45].

Modality compensation represents a VI ReID paradigm that initially employs a Generative Adversarial Network (GAN) [11] to generate another modality from the available one, then compensates the original image with the generated image, to mitigate the modality discrepancy. The cmGAN and D2RL [7, 39] are typical methodologies via modality compensation. Liu et al. [23] proposed a Deep Jump Connection Generative Adversarial Network (DS-GAN) to address the poor quality of generated images. In contrast to modality compensation methods [7, 23, 37, 39], several methods leverage shared backbone to extract discriminative modality-invariant features from images of different modalities. The goal is to eliminate modality-specific information and thereby reduce the modality discrepancy. Chen et al. [3] proposed to model the modality invariant structural features of each modality, and use the information of human body structure and part position to learn discriminative cross-modality invariant features at the part level. Liang et al. [21] innovatively proposed to design modality embeddings for the ViT [9] backbone and applied pure transformer [35] networks to VI ReID task for the first time. Existing methods [3, 37] involve complex and computationally intensive feature alignment and fusion operations to address modality discrepancies. Some approaches [20, 26] normalize or optimize the training process to eliminate interference from modality-specific information on shared feature learning. For example, Lu et al. [26] introduced grayscale images as auxiliary modalities and proposed a progressive learning strategy to help extract invariant features. However, it is worth noting that modality-specific information may still contain discriminative details that are beneficial for VI ReID.

### 2.3 Visual Prompt Learning

Inspired by the success of textual prompts [2, 19] in NLP, visual prompt learning has been widely used in several computer vision tasks. VPT [15] designed a set of learnable vectors prepended to the input sequence of each encoder layer, thereby achieving better or equivalent results on 24 downstream recognition benchmarks. Bahng et al. [1] proposed to construct prompt in the form of perturbations, exploring the use of visual prompt guiding the large-scale language model CLIP [33] to adapt to downstream tasks. Chen et al. [4] proposed to introduce learnable parameters into the pre-trained model for adapting to other downstream tasks, but different from the VPT, the learnable parameters are added to the transformer MLP layers rather than to the input sequence. Yang et al. [44] and Zhu et al. [54] incorporated prompt learning into the multi-modality track field, showcasing its efficacy in multi-modality tasks. Yu et al. [50] and Liu et al. [24] attempted to apply prompt in UDA ReID and DG ReID, respectively. These studies have demonstrated the potential of visual prompt learning in adapting original models to other tasks, but there is still no method to introduce visual prompt learning into the VI ReID field. In this work, we attempt to use specific prompts for different modality inputs and different instances to explore the application of visual prompt learning in the VI ReID.

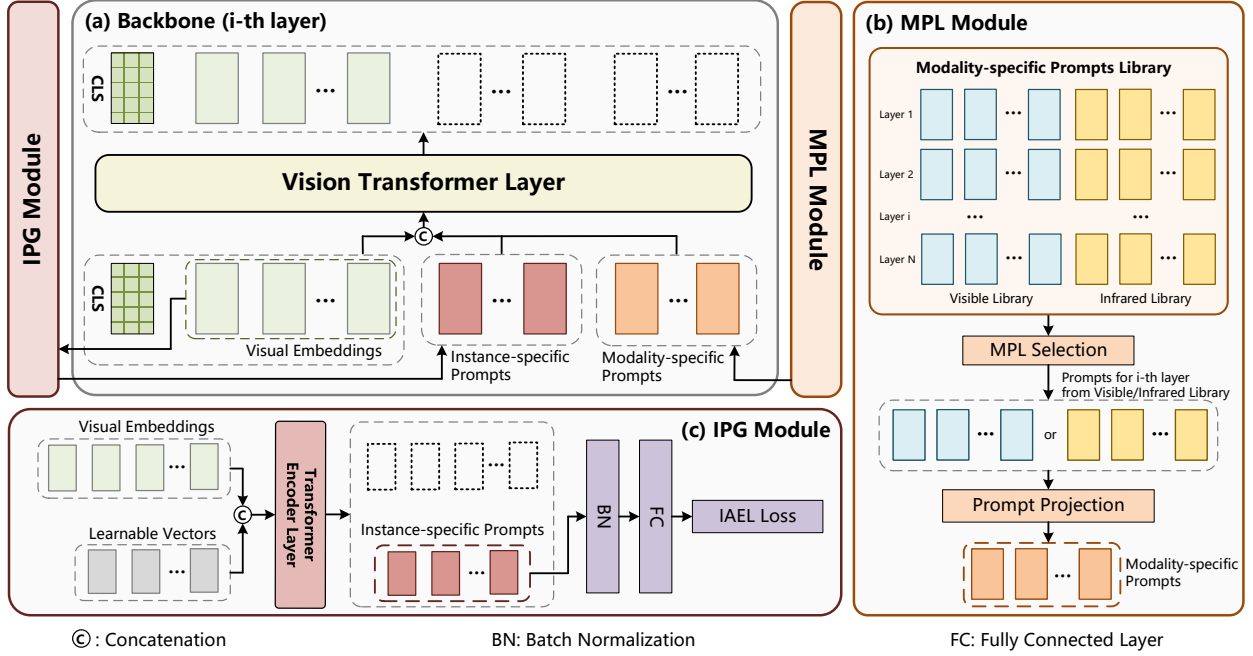


**Figure 2: The overall framework of our proposed MIP network, which consists of a backbone model and two major modules. (a) A pre-trained vision transformer [9] is used as the backbone model. (b) Modality-aware Prompts Learning (MPL) module produces modality-specific prompts for input visual embeddings of each layer according to the modality labels of input images. (c) Instance-aware Prompts Generator (IPG) module generates instance-specific prompts, and the generated prompts are supervised by "IAEL loss". The "IAEL Loss" is our proposed Instance-aware Enhancement Loss. The two kinds of prompts help the backbone network to adapt to different modality and instance inputs.**

### 3 APPROACH

In this section, we give the details of our proposed Modality-aware and Instance-aware Visual Prompts (MIP) network. Firstly, we briefly introduce the overall framework of MIP. Thereafter, the major components of MIP, namely, the Modality-aware Prompt Learning (MPL) module and the Instance-aware Prompt Generator (IPG) module, are illustrated in sequence. Finally, we give the introduction of the objective functions employed in model training.

#### 3.1 Preliminary

Our approach is built upon transformer architecture. In VI ReID, for an input image, we denote it as  $x^m \in \mathbb{R}^{C \times H \times W}$ , where the  $C, H, W$  denote channel dimension, height, width of the images, and  $m \in \{vis, ir\}$  denotes its modality flag. For each input image  $x^m$ , we split it into a patch sequence  $s^m \in \mathbb{R}^{l \times C \times b \times b}$ , where  $l$  denotes the length of the sequence and  $b$  denotes the size of the patch. Then,  $s^m$  is converted to image embedding  $e_0^m \in \mathbb{R}^{l \times D}$  by a linear projection layer, where  $D$  denotes the embedding dimension. Thereafter, an extra learnable class token  $a_0$  will be concatenated with the embedding  $e_0^m$ , and  $[a_0, e_0^m]$  will be sent into the transformer encoder layers as the initial input before the first layer, where  $[\cdot]$  indicates the concatenation operation. Additionally, we denote the transformer encoder layers as  $\{L_i\}_{i=1}^N$ , where  $N$  is the number of transformer encoder layers. Subsequently, the feature extraction

stage of the  $i$ -th layer can be described as the following,

$$[a_{i+1}, e_{i+1}^m] = L_i[a_i, e_i^m] \quad (1)$$

where  $a_{i+1}$  and  $e_{i+1}^m$  denote the output class token and the output embedding of the  $i$ -th layer and  $i = 1, \dots, N$ .

#### 3.2 Overall Framework

In this paper, we introduce a MIP network designed for the VI ReID task. Our primary focus is on adapting the model to different modality inputs and instance inputs, thereby mining the correspondences between different modalities/instances to facilitate VI ReID. We achieve these goals by employing two distinct sets of visual prompts. Specifically, we produce modality-specific prompts and instance-specific prompts according to current modality and instance input, and these two sets of prompts are concatenated after the feature embedding. By making use of modality-specific and instance-specific information preserved in these prompts, the model can explore potential correspondences between different modalities and instances, thereby facilitating the VI ReID.

The overall framework of our MIP is depicted in Figure 2. As shown in Figure 2, we use a vision transformer pre-trained on ImageNet [8] as the backbone and insert our designed modules, namely the Modality-aware Prompt Learning (MPL) module and the Instance-aware Prompt Generator (IPG) module, into the backbone model. These two proposed modules are responsible for capturing modality-specific and instance-specific information, and then

producing modality-specific and instance-specific visual prompts, respectively. Then, the visual prompts will be concatenated with the input before each transformer encoder layer, like the following,

$$[a_{i+1}, e_{i+1}^m, \_] = L_i[a_i, e_i^m, p_i] \quad (2)$$

$$p_i = [p_i^M, p_i^I] \quad (3)$$

where  $p = [p_i^M, p_i^I]$  is the visual prompts, and the composition of modality-specific prompts  $p_i^M$  and instance-specific  $p_i^I$  will be specifically explained in sections 3.3 and 3.4;  $L_i$  means the  $i$ -th transformer encoder layer and  $i = 1, \dots, N$ ; the  $\_$  is the output of  $p_i$ , which is discarded.

### 3.3 Modality-aware Prompt Learning

The existing methods alleviate the interference of the modality gap by simply focusing on modality-invariant information while eliminating modality-specific information, overlooking the potential utilization of modality-specific information. In this work, we notice that there could exist potential correspondences between modality-specific information, which could also assist re-identification. For an intuitive example, characteristics like clothing types/materials, discerned from visible images, could influence the heat radiation intensities, thereby impacting infrared brightness variations. Based on this idea, in this work, we attempt to guide the model to preserve and make use of modality-specific information. In this step, we notice that many studies [1, 4, 27, 44, 54], e.g., VPT [15] that achieved superior results across 24 downstream vision benchmarks, have demonstrated the potential of visual prompt learning in adapting original models to other tasks without complex operations and large extra computations, so we consider exploiting this advantage of prompt learning to help the model adapt to different modality inputs. We treat the adaptation of the model to visible and infrared modalities as two different tasks, applying two independent sets of learnable visual prompts for the two modalities, and also preserving the required modality-specific information. To achieve this, we propose an MPL module to produce modality-specific prompts, which is shown in Figure 2(b).

Formally, the MPL module initializes and maintains a modality-specific prompts library with a set of learnable vectors. The modality-specific prompts library can be written as  $P^M = \{p_i^{vis}, p_i^{ir}\}_{i=1}^N$ , in which  $N$  is the number of transformer encoder layers;  $p_i \in \mathbb{R}^{j \times D}$ ; the  $j$  is the length of the modality-specific prompt, in this case, we set  $j = 16$ ;  $p_i^{vis}$  and  $p_i^{ir}$  denote the visible-specific and infrared-specific prompts for the input before the  $i$ -th layer. Before the input embedding is sent into each encoder layer, the MPL module selects the target modality-specific prompt from the library according to the modality label of the image and the index of the layer to be input. The chosen modality-specific prompt will be concatenated with the input after being projected by a linear layer. The above processing can be written as,

$$\tilde{p}_i^M = \Gamma(P^M, m, i) \quad (4)$$

$$\Gamma(P^M, m, i) = \begin{cases} p_i^{vis} & , \text{if } m = vis \\ p_i^{ir} & , \text{if } m = ir \end{cases} \quad (5)$$

$$p_i^M = \varphi(\tilde{p}_i^M) \quad (6)$$

where  $i = 1, \dots, N$ ;  $\Gamma(\cdot)$  denotes the MPL Selection operation;  $\varphi(\cdot)$  denotes the prompt projection linear layer.

### 3.4 Instance-aware Prompt Generator

In addition to tailoring the model for different modalities and exploring implicit correspondences among modality-specific information, we also strive to customize our model for distinct instances by leveraging instance-specific prompts. The construction of instance-specific prompts is non-trivial. Here, we notice a great challenge, namely, we cannot train a set of independent prompts for each instance, because the test instances are unlimited and unpredictable. Therefore, in this work, we design a dynamic prompting module, capable of adaptively generating instance-specific prompts according to the input instance. To accomplish this, shown in Figure 2(c), we employ a transformer layer to transfer the instance-specific knowledge from the input image features into a group of learnable vectors. The outputs of these learnable vectors then serve as instance-specific prompts to adapt our model to various input instances.

Formally, given the input embedding  $e_i^m$  before the  $i$ -th layer, we employ a transformer encoder layer to transfer the information in the embedding  $e_i^m$  into a set of learnable vectors  $v_i \in \mathbb{R}^{k \times D}$ , where  $i = 1, \dots, N$ , and  $k$  is the length of the instance-specific prompt, which is set as  $k = 16$  in this work. The process of constructing instance-specific prompt can be written as follows,

$$[p_i^I, \_] = \text{Trans}([v_i, e_i^m]) \quad (7)$$

where the  $p_i^I$  is the output of  $v_i$ , i.e., instance-specific prompt; the  $\text{Trans}(\cdot)$  is a transformer encoder layer; the  $\_$  is the output of  $e_i^m$ , which is discarded.

### 3.5 Objective Function

We employ our designed Instance-aware Enhancement Loss (IAEL) and some losses commonly used in ReID tasks for our model.

**Instance-aware Enhancement Loss.** In practice, we observe that the modality-specific and instance-specific prompts are not easy to optimize. Particularly, the instance-specific prompts may degenerate to only get a trivial solution, which means it could be invariant to different instances while failing to be customized to them. To ensure that instance-specific prompts are indeed instance-customized, we have designed the IPG module in a generation-based manner rather than fusion-based ones like previous work [40], and we additionally designed a loss function called Instance Aware Enhancement Loss (IAEL) to force the generated prompts being instance-adaptive. The IAEL loss can be written formally as follows,

$$L_{IAEL} = - \sum_{i=1}^N y \cdot \log(\psi_i(\sigma_i(p_i^I))) \quad (8)$$

where  $i = 1, \dots, N$  means for the  $i$ -th layer;  $y$  is the ground-truth label of current input instance;  $\psi_i(\cdot)$  denotes the classifier for instance-specific prompts before the  $i$ -th layer;  $\sigma_i(\cdot)$  denotes Batch Normalization [14] layer.

**Overall Objective Function.** For model training, we adopt a hybrid loss function for our progressive learning framework. At the first stage, we utilize Cross-Entropy Loss  $L_{ID}$  and Triplet Loss

$L_{TRI}$ ,

$$L_1 = L_{ID} + L_{TRI} \quad (9)$$

In the second stage, we further extract the reliable features with  $L_{IAEL}$ . The loss function can be defined as,

$$L = \alpha_1 L_1 + \alpha_2 L_{IAEL} \quad (10)$$

where the parameters  $\alpha_1$  and  $\alpha_2$  are hyperparameters, and we set  $\alpha_1 = 1.0$  and  $\alpha_2 = 0.5$ . In practice, the model performs stably, and using different hyperparameters does not result in significant performance changes.

## 4 EXPERIMENT

In this section, we conduct comprehensive experiments to verify the superiority of our Modality-aware and Instance-aware Visual Prompts (MIP) network for VI ReID.

### 4.1 Datasets and Evaluation Protocols

Two mainstream public VI ReID datasets, SYSU-MM01 and RedDB, are used for our experiments.

**SYSU-MM01** [41] consists of 491 persons whose 286,628 visible and 15,792 infrared images are captured by 4 visible and 2 infrared cameras. The dataset is divided into the training set and the test set. There are 22,258 visible images and 11,909 infrared images of 395 persons in the training set, and the test set contains images of 96 persons whose 3,803 infrared images are used as query images and several visible images are randomly selected as gallery images. According to the general setting, the composition of gallery images is decided by two search modes: *All-Search* and *Indoor-Search*, and two selection modes: *Single-Shot* and *Multi-Shot*. In *All-Search* mode, images under all visible cameras can be selected, while in *Indoor-Search* mode, only images under indoor visible cameras can be selected for gallery images. And 1 image is selected for each person in *Single-Shot* mode, and 10 images are selected for each person in *Multi-Shot* mode.

**RegDB** [29] consists of 412 persons whose 4,120 visible and 4,120 infrared images are captured by one visible camera and one infrared camera, and there are 10 visible and 10 infrared images for each person. The training set includes the images of 206 randomly chosen persons and the test set contains the images of the remaining 206 persons. In the test mode *Visible to Infrared*, the visible images are used as query images, and the infrared images are used as gallery images, and the arrangement is reversed in *Infrared to Visible* mode.

**Evaluation Protocols.** We adopt the Cumulative Matching Characteristic curve (CMC) and mean Average Precision (mAP) as the evaluation metrics on the two datasets, to quantitatively evaluate the performance of our proposed model. For CMC, we calculate the percentage of correctly retrieved images among top-1 results (Rank-1 accuracy) based on similarity.

### 4.2 Implementation Details

Our proposed MIP method is implemented on the Pytorch framework, and one NVIDIA RTX3090 GPU is used to execute all experiments. In our experiments, we use a vision transformer [9] pre-trained on ImageNet [8] as the backbone. During training, the input images are resized to  $256 \times 128$ , and the data augmentations, including random cropping, color jittering, random erasing, and

grayscale, are applied to transform the input images. The batch size is set to  $4 (\text{persons}) \times (8 (\text{visible images}) + 8 (\text{infrared images})) = 64$ . We adopt the Stochastic Gradient Descent (SGD) optimizer to train the model for 80 epochs with an initial learning rate of  $1.0 \times 10^{-2}$ . The learning rate will decay with the cosine decay schedule, where the minimum learning rate is  $1.0 \times 10^{-5}$ , the momentum parameter is 0.9, and the decay rate is 0.1. Following the framework of Figure 2, we maintain two sets of modality-specific prompts for each layer and a shared IPG module for all layers. This results in 7.67% and 4.09% extra parameters, respectively.

### 4.3 Comparison with State-of-the-art methods

We compare our MIP with existing state-of-the-art methods for VI ReID, in mainstream datasets SYSU-MM01 and RegDB. The comparison results are reported in Table 1, where bold and underlined fonts indicate the best and second-best performance, respectively.

**SYSU-MM01:** We can observe that our proposed MIP method shows the best results on all the metrics under all SYSU-MM01 dataset modes. Compared with other transformer-based methods, PMT, CMTR, DFLN-ViT, SPOT [3] and recent CNN-based method TOPLight [49], our MIP outperforms the state-of-the-art results by 3.31%/5.91% Rank-1 and 1.43%/3.22% mAP under the *All-Search/Indoor-Search + Single-Shot* mode. Recent other methods are lacking rich experiments under changeable *Multi-Shot* mode, and MIP still achieves better results than CMTR with an improvement of 2.69%/2.29% Rank-1 and 1.42%/1.16% mAP.

**RegDB:** As shown in Table 1, our proposed MIP method also achieves promising performance on RegDB. Compared with other top-performing methods, MIP outperforms the state-of-the-art results by 1.17% Rank-1 and 2.13% mAP under *Infrared to Visible* mode. MIP also outperforms the state-of-the-art result by 1.05% mAP under *Visible to Infrared* mode, but DFLN-ViT shows the best Rank-1 result of 92.10%, while MIP also shows a comparable Rank-1 result of 91.26% and outperforms by 3.79% mAP. The main reason for DFLN-ViT’s better result could be that its structure-aware mechanism can model align persons’ structures easily on simple images in RegDB. But this kind of method is viewpoint sensitive, and its performance on SYSU-MM01 with complex viewpoint changes is 11.89% lower than MIP on average.

### 4.4 Ablation Studies

In this subsection, we conduct a series of ablation experiments to evaluate the effectiveness of our proposed MIP. We begin by validating the effectiveness of each component. Next, we compare our carefully designed MPL and IPG modules with general prompt-based approaches. Subsequently, we discuss the necessity of the generation-based design of the IPG module. Finally, we present the effect of the MPL module on extracting implicit correspondence between modality-specific information. Notably, all the ablation experiments are conducted on the SYSU-MM01 dataset under *Single-Shot* mode, except when specifically stated.

**Effectiveness of Proposed Components.** To evaluate the effectiveness of our proposed MPL module, IPG module, and IAEL loss, we add these three components to the baseline gradually and evaluate the performances. As shown in Table 2, compared with

**Table 1: The experiment results of our MIP and other state-of-the-art methods under various test modes of SYSU-MM01 and RegDB datasets. Summarily, our proposed MIP outperforms other state-of-the-art methods on both two mainstream datasets.**

Methods	Reference	SYSU-MM01								RegDB			
		All-Search				Indoor-Search				Infrared to Visible		Visible to Infrared	
		Single-Shot		Multi-Shot		Single-Shot		Multi-Shot		Rank-1	mAP	Rank-1	mAP
		Rank-1	mAP	Rank-1	mAP	Rank-1	mAP	Rank-1	mAP	Rank-1	mAP	Rank-1	mAP
Zero-Pad [41]	ICCV'17	14.80	15.95	19.13	10.89	20.58	26.92	24.43	18.64	-	-	-	-
cmGAN [7]	IJCAI'18	26.97	27.80	31.49	22.27	31.63	42.19	37.00	32.76	-	-	-	-
AlignGAN [37]	ICCV'19	42.40	40.70	51.50	33.90	45.90	54.30	57.10	45.30	56.30	53.40	57.90	53.60
CMM+CML [22]	MM'20	51.80	51.21	56.27	43.39	54.98	63.70	60.42	53.52	59.81	60.86	-	-
DDAG [46]	ECCV'20	54.75	53.02	-	-	61.02	67.98	-	-	68.06	61.80	69.34	63.46
NFS [6]	CVPR'21	56.91	55.45	63.51	48.56	62.79	69.79	70.03	61.45	77.95	69.79	80.54	72.10
CM-NAS [10]	ICCV'21	61.99	60.02	68.68	53.45	-	-	-	-	84.54	80.32	82.57	78.31
AGW [47]	TPAMI'21	47.50	47.65	-	-	54.17	62.97	-	-	-	-	70.05	66.37
MID [13]	AAAI'22	60.27	59.40	-	-	64.86	70.12	-	-	84.29	81.41	87.45	84.85
FMCNet [51]	CVPR'22	66.34	62.51	-	-	68.15	74.09	-	-	88.38	83.86	89.12	84.43
SPOT [3]	TIP'22	65.34	62.25	-	-	69.42	74.63	-	-	79.37	72.26	80.35	72.46
PMT [26]	AAAI'23	<u>67.53</u>	<u>64.98</u>	-	-	71.66	76.52	-	-	84.16	75.13	84.83	76.55
TOPLight [49]	CVPR'23	66.76	64.01	-	-	<u>72.89</u>	<u>76.70</u>	-	-	80.65	75.91	85.51	79.95
CMTR [21]	TMM'23	65.45	62.90	<u>71.99</u>	<u>57.07</u>	71.46	76.67	<u>80.00</u>	<u>69.49</u>	84.92	80.79	88.11	81.66
DFLN-ViT [52]	TMM'23	59.54	57.70	-	-	62.13	69.03	-	-	91.21	81.62	<b>92.10</b>	82.11
<b>OURS</b>	-	<b>70.84</b>	<b>66.41</b>	<b>74.68</b>	<b>58.49</b>	<b>78.80</b>	<b>79.92</b>	<b>82.29</b>	<b>70.65</b>	<b>92.38</b>	<b>85.99</b>	91.26	<b>85.90</b>

Method-1, i.e., baseline model, Method-2 is trained with an additional MPL module, which brings a significant improvement of 22.44% mAP and 27.40% Rank-1 on average under two search modes on SYSU-MM01 dataset. Meanwhile, Method-3 adopts baseline+IPG as the model and improves the performance of the baseline model by 14.23% mAP and 16.44% Rank-1 on average on SYSU-MM01. Based on Method-3, Method-4 adds IAEL loss to promote the prompt generated by the IPG module to be more customized to each input instance, achieving an average improvement of 2.59% mAP and 3.44% Rank-1 compared with Method-3. What's more, Method-5 equips the baseline with both MPL and IPG modules, which brings a further improvement of 8.30% mAP and 9.04% Rank-1 on average than baseline+MPL and baseline+IPG. This indicates that our designed modules can complement to jointly promote performance improvement. Finally, Method-6, our full model (MIP), achieves an additional average improvement of 1.51% in mAP and 2.74% in Rank-1 compared to Method-5, thanks to the enhancement from the IAEL loss. We also conduct the same ablation experiments on the RegDB dataset, as shown in Table 3, and the addition of individual components similarly brings performance improvements to the model. From these experiments, we can find that the MPL module, IPG modules, and IAEL Loss are effective in adapting the model to different modalities and instances and enhancing its capability for VI ReID.

**Comparisons with General Prompt-based Approaches.** Several prompt-based approaches [1, 4, 15, 27, 44, 54] have demonstrated the ability of visual prompt learning in adapting original models to various tasks. To explore whether the advantages of MPL and IPG modules solely depend on effective visual prompts learning, the modules designed in MIP are replaced with general prompts learning [15], and the experiments are repeated, results of which are shown in Table 4.

**Table 2: The effects of our proposed components performed on SYSU-MM01.**

Methods	Components			All-Search		Indoor-Search	
	MPL	IPG	IAEL	Rank-1	mAP	Rank-1	mAP
1(Base)				40.49	40.93	41.76	49.12
2	✓			63.77	60.10	73.28	74.83
3		✓		52.98	52.75	62.14	65.75
4		✓	✓	55.48	54.81	66.53	68.87
5	✓	✓		67.21	64.35	76.95	78.95
<b>6(Full)</b>	<b>✓</b>	<b>✓</b>	<b>✓</b>	<b>70.84</b>	<b>66.41</b>	<b>78.80</b>	<b>79.92</b>

**Table 3: The effects of our proposed components performed on RegDB.**

Methods	Components			Infrared to Visible		Visible to Infrared	
	MPL	IPG	IAEL	Rank-1	mAP	Rank-1	mAP
1(Base)				87.14	80.20	85.05	79.16
2	✓			88.64	82.89	89.81	82.27
3		✓		88.70	83.20	89.50	82.80
4		✓	✓	89.85	84.05	89.90	83.47
5	✓	✓		91.26	85.43	91.17	84.86
<b>6(Full)</b>	<b>✓</b>	<b>✓</b>	<b>✓</b>	<b>91.26</b>	<b>85.90</b>	<b>92.38</b>	<b>85.99</b>

As shown in Table 4, Method-2, i.e., baseline+general-prompts, only improves performance with an average increase of 5.58% mAP and 8.55% Rank-1 compared to the baseline model. In contrast, in Method-3 and Method-4, we replace the general prompts learning with our designed MPL module and IPG module, introducing significant improvements to Method-2, i.e., 16.86/8.65% mAP and 18.85/7.89% Rank-1 on average, respectively. This result illustrates

**Table 4: The effects of our designed MPL and IPG modules compared with general prompt-based approaches. The "✓✓" means using two sets of general prompts to replace modality-specific and instance-specific prompts, respectively.**

Methods	Prompts			All-Search		Indoor-Search	
	General	MPL	IPG	Rank-1	mAP	Rank-1	mAP
1(Base)				40.49	40.93	41.76	49.12
2	✓			44.73	42.73	54.62	58.48
3		✓		63.77	60.10	73.28	74.83
4			✓	52.98	52.75	62.14	65.75
5	✓✓			51.70	47.44	57.29	60.17
6		✓	✓	67.21	64.35	76.95	78.95

**Table 5: The comparisons of generation-based and fusion-based IPG modules.**

Methods	IPG		IAEL	MPL	All-Search		Indoor-Search	
	Fusion	Generation			Rank-1	mAP	Rank-1	mAP
1(Base)					40.49	40.93	41.76	49.12
2	✓				54.17	50.01	62.73	64.42
3		✓			52.98	52.75	62.14	65.75
4	✓		✓		56.30	52.87	67.98	69.27
5		✓			55.48	54.81	66.53	68.87
6					63.77	60.10	73.28	74.83
7	✓				63.00	59.86	74.05	74.98
8		✓		✓	67.21	64.35	76.95	78.95
9	✓		✓		63.11	59.90	73.19	74.49
10(Full)		✓	✓		<b>70.84</b>	<b>66.41</b>	<b>78.80</b>	<b>79.92</b>

the necessity to design specifically for modality and instance adaptation. Furthermore, the performance of Method-6 equipped with both MPL and IPG is 17.85% higher in mAP and 17.59% higher in Rank-1 than Method-5 using two sets of general prompts, which achieves more obvious advantages than that when only equipped with a single module.

The above ablation experiments could denote that the improvement brought by MPL and IPG modules for VI ReID tasks is not solely dependent on the effectiveness of visual prompt learning. We illustrate the necessity of carefully designing these two modules to help the model adapt to different modalities and different instances and the necessity of capturing modality-specific and instance-specific information to mine potential relationships.

**Ablation about the product strategy of instance-specific prompts.** Unlike our generation-based strategy, previous work [40] proposes a fusion-based instance-specific prompt learning pipeline. This pipeline generates specific weights for each input instance, which are then used to fuse several prompt prototypes and create instance-specific prompts. To validate the necessity of our generation-based strategy, we implement a fusion-based IPG module and conduct several experiments to compare it with our generation-based IPG module.

As shown in Table 5, Method-7, which adds a fusion-based IPG module to Method-6, does not show additional improvement over Method-6. In contrast, Method-8, which adds a generation-based IPG module to Method-6, demonstrates a significant improvement. After introducing the IAEL loss, comparing Method-6, Method-9, and Method-10 in Table 5, we can also get a similar finding. In addition, Method-1 to Method-5 show the results without the MPL

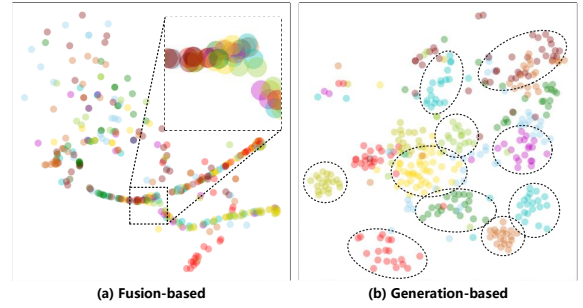


**Figure 3: The t-SNE visualizations results of prompts from fusion-based and generation-based IPG modules. Different colors represent distinct identities. (a) Fusion-based IPG prompts cluster closely, with less obvious boundaries between individuals, indicating weaker instance-aware ability. (b) Generation-based IPG prompts show increased distances between individuals, reflecting stronger instance-aware ability, crucial for effective adaptation to diverse instances.**

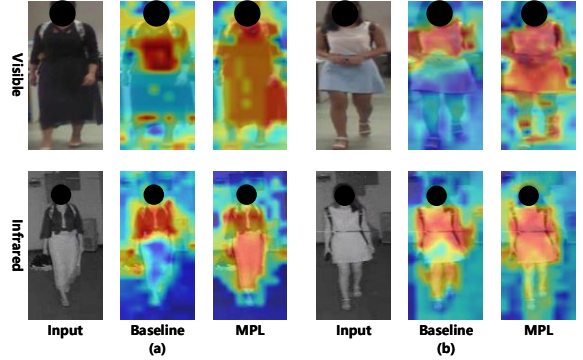


**Figure 4: The visualizations results of attention maps of our MPL module and baseline model. From the second column in each case, we could find that the baseline model tends only to capture the explicit correspondence between different modality inputs. Such as only focusing on the upper dress part while ignoring the skirt part in case (a). As for our MPL module, with the carefully designed modality-specific prompts, it could effectively adapt to and make use of the modality-specific information. This enables our MPL model to explore and capture the implicit correspondence between the skirts part. Case (b) shows a similar result.**

module. We can find that the fusion-based IPG module brings an average improvement of 12.19% mAP and 17.33% Rank-1 to the baseline when it does not work with the MPL module. However, its improvement of mAP is still 2.04% lower than the improvement brought by the generation-based IPG module on average. The results are similar after introducing the IAEL loss. The reason behind this could be that, the awareness ability of prompts generated by the fusion-based IPG module may not be strong enough because of degenerating to the trivial solution. Consequently, when the two modules work together, the fusion-based IPG module might duplicate the role of the MPL module.



To intuitively explore this finding, we exhibit the t-SNE visualization results of instance-specific prompts produced by fusion-based and generation-based IPG modules in Figure 3. We randomly sample 386 images of 10 different persons. The different colors of dots mean different persons. As shown in Figure 3, the prompts produced by generation-based IPG have obvious intra-person distances and clear boundaries, while the prompts generated by the fusion-based IPG are distributed in a disordered and interleaving manner, which indicates that prompts produced by generation-based IPG have more fine-grained instance-aware ability than prompts produced by fusion-based IPG.

**Focused Contents of the MPL Module.** We present some visualization cases to further analyze what the MPL module focuses on and determine if MPL does extract the implicit correspondence between modality-specific information. As shown in Figure 4, we generate the attention maps of some case images in baseline and model with the MPL module. Taking case (a) in Figure 4 as an example, as shown in the first column, the color and brightness of skirts presented in different modalities are significantly different. Therefore, from the second column, we find that the baseline model tends to only capture the explicit correspondence between different modality inputs, thereby focusing only on the upper dress part while ignoring the skirt part. As for our MPL module, with the carefully designed modality-specific prompts, it could effectively adapt to and make use of the modality-specific information. This enables our MPL model to explore and capture the implicit correspondence between the skirts part. This is consistent with our motivation, and case (b) shows a similar result.

## 5 CONCLUSION

In this work, we propose a novel VI ReID method, the Modality-aware and Instance-aware Visual Prompts (MIP) network, which incorporates visual prompt learning into the VI ReID field. We design a Modality-aware Prompt Learning (MPL) module and an Instance-aware Prompt Generator (IPG) to generate modality-specific and instance-specific prompts for the ReID model, which guides the model to adapt to inputs of different modalities and leverage modality-specific information, and capture identity-specific discriminative clues that help re-identification, respectively. We anticipate that this work will serve as a catalyst for future research exploring the significance of modality-specific and instance-specific information in VI ReID.

## ACKNOWLEDGMENTS

This work was supported by the National Natural Science Foundation of China (No.U23B2013), the Shaanxi Provincial Key R&D Program (No.2021KWZ-03, No.2024GX-YBXM-117), and the Natural Science Basic Research Program of Shaanxi (No.2021JCW-03).

## REFERENCES

- [1] Hyojin Bahng, Ali Jahanian, Swami Sankaranarayanan, and Phillip Isola. 2022. Exploring Visual Prompts for Adapting Large-Scale Models. *arXiv preprint arXiv:2203.17274* (2022).
- [2] Tom Brown, Benjamin Mann, Nick Ryder, Melanie Subbiah, Jared D Kaplan, Prafulla Dhariwal, Arvind Neelakantan, Pranav Shyam, Girish Sastry, Amanda Askell, et al. 2020. Language models are few-shot learners. *Advances in neural information processing systems* 33 (2020), 1877–1901.
- [3] Cuiqun Chen, Mang Ye, Meibin Qi, Jingjing Wu, Jianguo Jiang, and Chia-Wen Lin. 2022. Structure-Aware Positional Transformer for Visible-Infrared Person Re-Identification. *IEEE Trans. Image Process.* 31 (2022), 2352–2364.
- [4] Shoufa Chen, Chongjian GE, Zhan Tong, Jiangliu Wang, Yibing Song, Jue Wang, and Ping Luo. 2022. AdaptFormer: Adapting Vision Transformers for Scalable Visual Recognition. In *Proc. Advances in Neural Inf. Process. Syst.*, Vol. 35. 16664–16678.
- [5] Weihua Chen, Xiaotang Chen, Jianguo Zhang, and Kaiqi Huang. 2017. Beyond Triplet Loss: A Deep Quadruplet Network for Person Re-identification. In *Proc. IEEE Conf. Comp. Vis. Patt. Recogn.* 1320–1329.
- [6] Yehansen Chen, Lin Wan, Zhihang Li, Qianyan Jing, and Zongyuan Sun. 2021. Neural Feature Search for RGB-Infrared Person Re-Identification. In *Proc. IEEE Conf. Comp. Vis. Patt. Recogn.* 587–597.
- [7] Pingyang Dai, Rongrong Ji, Haibin Wang, Qiong Wu, and Yuyu Huang. 2018. Cross-Modality Person Re-Identification with Generative Adversarial Training. In *Proc. Int. Joint Conf. Artificial Intell.* 677–683.
- [8] Jia Deng, Wei Dong, Richard Socher, Li-Jia Li, Kai Li, and Li Fei-Fei. 2009. ImageNet: A large-scale hierarchical image database. In *Proc. IEEE Conf. Comp. Vis. Patt. Recogn.* 248–255.
- [9] Alexey Dosovitskiy, Lucas Beyer, Alexander Kolesnikov, Dirk Weissenborn, Xiuhua Zhai, Thomas Unterthiner, Mostafa Dehghani, Matthias Minderer, Georg Heigold, Sylvain Gelly, et al. 2020. An image is worth 16x16 words: Transformers for image recognition at scale. *arXiv preprint arXiv:2010.11929* (2020).
- [10] Chaoyou Fu, Yibo Hu, Xiang Wu, Hailin Shi, Tao Mei, and Ran He. 2021. CM-NAS: Cross-Modality Neural Architecture Search for Visible-Infrared Person Re-Identification. In *Proc. IEEE Int. Conf. Comp. Vis.* 11803–11812.
- [11] Ian Goodfellow, Jean Pouget-Abadie, Mehdi Mirza, Bing Xu, David Warde-Farley, Sherjil Ozair, Aaron Courville, and Yoshua Bengio. 2014. Generative Adversarial Nets. In *Proc. Advances in Neural Inf. Process. Syst.*, Vol. 27.
- [12] Alexander Hermans, Lucas Beyer, and Bastian Leibe. 2017. In Defense of the Triplet Loss for Person Re-Identification. *arXiv preprint arXiv:1703.07737* (2017).
- [13] Zhipeng Huang, Jiawei Liu, Liang Li, Kecheng Zheng, and Zheng-Jun Zha. 2022. Modality-Adaptive Mixup and Invariant Decomposition for RGB-Infrared Person Re-identification. In *Proc. Conf. AAAI*. 1034–1042.
- [14] Sergey Ioffe and Christian Szegedy. 2015. Batch normalization: accelerating deep network training by reducing internal covariate shift. In *Proc. Int. Conf. Mach. Learn.* 448–456.
- [15] Menglin Jia, Luming Tang, Bor-Chun Chen, Claire Cardie, Serge Belongie, Bharath Hariharan, and Ser-Nam Lim. 2022. Visual prompt tuning. In *Proc. Eur. Conf. Comp. Vis.* Springer, 709–727.
- [16] Bingliang Jiao, Lingqiao Liu, Liying Gao, Guosheng Lin, Ruiqi Wu, Shizhou Zhang, Peng Wang, and Yanning Zhang. 2022. Generalizable Person Re-Identification via Viewpoint Alignment and Fusion. *arXiv preprint arXiv:2212.02398* (2022).
- [17] Bingliang Jiao, Lingqiao Liu, Liying Gao, Guosheng Lin, Lu Yang, Shizhou Zhang, Peng Wang, and Yanning Zhang. 2022. Dynamically Transformed Instance Normalization Network for Generalizable Person Re-Identification. In *Proc. Eur. Conf. Comp. Vis.*
- [18] Bingliang Jiao, Lingqiao Liu, Liying Gao, Ruiqi Wu, Guosheng Lin, Peng Wang, and Yanning Zhang. 2023. Toward Re-Identifying Any Animal. In *Proc. Advances in Neural Inf. Process. Syst.*
- [19] Brian Lester, Rami Al-Rfou, and Noah Constant. 2021. The power of scale for parameter-efficient prompt tuning. In *Proc. Conf. Empirical Methods in Natural Language Processing*. 3045–3059.
- [20] Wenkang Li, Ke Qi, Wenbin Chen, and Yicong Zhou. 2021. Bridging the Distribution Gap of Visible-Infrared Person Re-identification with Modality Batch Normalization. In *Proc. Int. Conf. on Artificial Intelligence and Computer Applications*. 23–28.
- [21] Tengfei Liang, Yi Jin, Wu Liu, and Yidong Li. 2023. Cross-Modality Transformer With Modality Mining for Visible-Infrared Person Re-Identification. *IEEE Trans. Multimedia* (2023), 1–13.
- [22] Yongguo Ling, Zhun Zhong, Zhiming Luo, Paolo Rota, Shaozi Li, and Nicu Sebe. 2020. Class-Aware Modality Mix and Center-Guided Metric Learning for Visible-Thermal Person Re-Identification. In *ACM Int. Conf. Multimedia*. 889–897.
- [23] Jianan Liu, Jialiang Wang, Nianchang Huang, Qiang Zhang, and Jungong Han. 2022. Revisiting Modality-Specific Feature Compensation for Visible-Infrared Person Re-Identification. *IEEE Trans. Circuits Syst. Video Technol.* 32, 10 (2022), 7226–7240.
- [24] Jialu Liu and Meng Yang. 2023. Prompt-Based Transformer for Generalizable Person Re-identification with Image Masking. In *Chinese Conference on Biometric Recognition*. 259–268.
- [25] Xinchun Liu, Wu Liu, Huadong Ma, and Huiyuan Fu. 2016. Large-scale vehicle re-identification in urban surveillance videos. In *Proc. IEEE Int. Conf. Multimedia Expo*. 1–6.
- [26] Hu Lu, Xuezhong Zou, and Pingping Zhang. 2023. Learning Progressive Modality-Shared Transformers for Effective Visible-Infrared Person Re-Identification. In *Proc. Conf. AAAI*. 1835–1843.
- [27] Yunxin Lu, Jianzhuang Liu, Yonggang Zhang, Yajing Liu, and Xinmei Tian. 2022. Prompt Distribution Learning. In *Proc. IEEE Conf. Comp. Vis. Patt. Recogn.* 5196–5205.
- [28] Hao Luo, Wei Jiang, Youzhi Gu, Fuxu Liu, Xingyu Liao, Shenqi Lai, and Jianyang Gu. 2020. A Strong Baseline and Batch Normalization Neck for Deep Person Re-Identification. *IEEE Trans. Multimedia* 22, 10 (2020), 2597–2609.
- [29] Dat Tien Nguyen, Hyung Gil Hong, Ki Wan Kim, and Kang Ryoung Park. 2017. Person Recognition System Based on a Combination of Body Images from Visible Light and Thermal Cameras. *Sensors* 17 (2017), 605.
- [30] Yuxin Peng, Jinwei Qi, and Yuxin Yuan. 2018. Modality-Specific Cross-Modal Similarity Measurement With Recurrent Attention Network. *IEEE Transactions on Image Processing* 27, 11 (2018), 5585–5599.
- [31] Xuelin Qian, Yanwei Fu, Tao Xiang, Wenxuan Wang, Jie Qiu, Yang Wu, Yu-Gang Jiang, and Xiangyang Xue. 2018. Pose-normalized image generation for person re-identification. In *Proceedings of the European conference on computer vision*. 650–667.
- [32] Xuelin Qian, Wenxuan Wang, Li Zhang, Fangrui Zhu, Yanwei Fu, Tao Xiang, Yu-Gang Jiang, and Xiangyang Xue. 2020. Long-term cloth-changing person re-identification. In *Proceedings of the Asian Conference on Computer Vision*.
- [33] Alec Radford, Jong Wook Kim, Chris Hallacy, Aditya Ramesh, Gabriel Goh, Sandhini Agarwal, Girish Sastry, Amanda Askell, Pamela Mishkin, Jack Clark, et al. 2021. Learning transferable visual models from natural language supervision. In *Proc. Int. Conf. Mach. Learn.* PMLR, 8748–8763.
- [34] Yifan Sun, Liang Zheng, Yi Yang, Qi Tian, and Shengjin Wang. 2018. Beyond Part Models: Person Retrieval with Refined Part Pooling (and A Strong Convolutional Baseline). In *Proc. Eur. Conf. Comp. Vis.* 501–518.
- [35] Ashish Vaswani, Noam Shazeer, Niki Parmar, Jakob Uszkoreit, Llion Jones, Aidan N Gomez, Łukasz Kaiser, and Illia Polosukhin. 2017. Attention is all you need. *Proc. Advances in Neural Inf. Process. Syst.* 30, 6000–6010.
- [36] Guanshuo Wang, Yufeng Yuan, Xiong Chen, Jiwei Li, and Xi Zhou. 2018. Learning Discriminative Features with Multiple Granularities for Person Re-Identification. In *ACM Int. Conf. Multimedia*. 274–282.
- [37] Guan'an Wang, Tianzhu Zhang, Jian Cheng, Si Liu, Yang Yang, and Zengguang Hou. 2019. RGB-Infrared Cross-Modality Person Re-Identification via Joint Pixel and Feature Alignment. In *Proc. IEEE Int. Conf. Comp. Vis.* 3622–3631.
- [38] Peng Wang, Bingliang Jiao, Lu Yang, Yifei Yang, Shizhou Zhang, Wei Wei, and Yanning Zhang. 2019. Vehicle re-identification in aerial imagery: Dataset and approach. In *Proc. IEEE Int. Conf. Comp. Vis.* 460–469.
- [39] Zhixiang Wang, Zheng Wang, Yinqiang Zheng, Yung-Yu Chuang, and Shin'ich Satoh. 2019. Learning to Reduce Dual-Level Discrepancy for Infrared-Visible Person Re-Identification. In *Proc. IEEE Conf. Comp. Vis. Patt. Recogn.* 618–626.
- [40] Zifeng Wang, Zizhao Zhang, Chen-Yu Lee, Han Zhang, Ruoxi Sun, Xiaoqi Ren, Guolong Su, Vincent Perot, Jennifer Dy, and Tomas Pfister. 2022. Learning to Prompt for Continual Learning. In *Proc. IEEE Conf. Comp. Vis. Patt. Recogn.* 139–149.
- [41] Ancong Wu, Wei-Shi Zheng, Hong-Xing Yu, Shaogang Gong, and Jianhuang Lai. 2017. RGB-Infrared Cross-Modality Person Re-identification. In *Proc. IEEE Int. Conf. Comp. Vis.* 5390–5399.
- [42] Fei Wu, Xiao-Yuan Jing, Zhiyong Wu, Yimu Ji, Xiwei Dong, Xiaokai Luo, Qinghua Huang, and Ruchuan Wang. 2020. Modality-specific and shared generative adversarial network for cross-modal retrieval. *Pattern Recogn.* 104 (2020), 107335.
- [43] Lin Wu, Yang Wang, Ling Shao, and Meng Wang. 2019. 3-D PersonVLAD: Learning Deep Global Representations for Video-Based Person Reidentification. *IEEE Transactions on Neural Networks and Learning Systems* 30, 11 (2019), 3347–3359.
- [44] Jinyu Yang, Zhe Li, Feng Zheng, Ales Leonardis, and Jingkuan Song. 2022. Prompting for Multi-Modal Tracking. In *ACM Int. Conf. Multimedia*. 3492–3500.
- [45] Mang Ye, Xiangyuan Lan, Zheng Wang, and Pong C. Yuen. 2020. Bi-Directional Center-Constrained Top-Ranking for Visible Thermal Person Re-Identification. *IEEE Transactions on Information Forensics and Security* 15 (2020), 407–419.
- [46] Mang Ye, Jianbing Shen, David J. Crandall, Ling Shao, and Jiebo Luo. 2020. Dynamic Dual-Attentive Aggregation Learning for Visible-Infrared Person Re-Identification. In *Proc. Eur. Conf. Comp. Vis.* 229–247.
- [47] Mang Ye, Jianbing Shen, Gaojie Lin, Tao Xiang, Ling Shao, and Steven C. H. Hoi. 2022. Deep Learning for Person Re-Identification: A Survey and Outlook. *IEEE Trans. Pattern Anal. Mach. Intell.* 44, 6 (2022), 2872–2893.
- [48] Dong Yi, Zhen Lei, Shengcai Liao, and Stan Z. Li. 2014. Deep Metric Learning for Person Re-identification. In *Proc. Int. Conf. Patt. Recogn.* 34–39.
- [49] Hao Yu, Xu Cheng, and Wei Peng. 2023. TOPLight: Lightweight Neural Networks with Task-Oriented Pretraining for Visible-Infrared Recognition. In *Proc. IEEE Conf. Comp. Vis. Patt. Recogn.* 3541–3550.

- [50] Shengming Yu, Zhaopeng Dou, and Shengjin Wang. 2023. Prompting and Tuning: A Two-Stage Unsupervised Domain Adaptive Person Re-identification Method on Vision Transformer Backbone. *Tsinghua Science and Technology* 28, 4 (2023), 799–810.
- [51] Qiang Zhang, Changzhou Lai, Jianan Liu, Nianchang Huang, and Jungong Han. 2022. FMCNet: Feature-Level Modality Compensation for Visible-Infrared Person Re-Identification. In *Proc. IEEE Conf. Comp. Vis. Patt. Recogn.* 7339–7348.
- [52] Jiaqi Zhao, Hanzheng Wang, Yong Zhou, Rui Yao, Silin Chen, and Abdulmotaleb El Saddik. 2023. Spatial-Channel Enhanced Transformer for Visible-Infrared Person Re-Identification. *IEEE Trans. Multimedia* 25 (2023), 3668–3680.
- [53] Liang Zheng, Liyue Shen, Lu Tian, Shengjin Wang, Jingdong Wang, and Qi Tian. 2015. Scalable person re-identification: A benchmark. In *Proc. IEEE Int. Conf. Comp. Vis.* 1116–1124.
- [54] Jiawen Zhu, Simiao Lai, Xin Chen, Dong Wang, and Huchuan Lu. 2023. Visual Prompt Multi-Modal Tracking. In *Proc. IEEE Conf. Comp. Vis. Patt. Recogn.* 9516–9526.